www.MaterialsViews.com

Monodisperse Emulsion Drop Microenvironments for Bacterial Biofilm Growth

*Connie B. Chang, James N. Wilking, Shin-Hyun Kim, Ho Cheung Shum, and David A. Weitz**

In this work, microfluidic technology is used to rapidly create hundreds of thousands of monodisperse double and triple emulsion drops that serve as 3D microenvironments for the containment and growth of bacterial biofilms. The size of these drops, with diameters from tens to hundreds of micrometers, makes them amenable to rapid manipulation and analysis. This is demonstrated by using microscopy to visualize cellular differentiation of Bacillus subtilis biofilm communities within each drop and the bacterial biofilm microstructure. Biofilm growth is explored upon specific interfaces in double and triple emulsions and upon negative and positive radii of curvature. Biofilm attachment of matrix and flagella mutants is studied as well as biofilms of Pseudomonas aeruginosa. This is the first demonstration of biofilms grown in microscale emulsion drops, which serve as both templates and containers for biofilm growth and attachment. These microenvironments have the potential to transform existing high-throughput screening methods for bacterial biofilms.

1. Introduction

Plaque formation on teeth, slime on contact lenses, and slippery sink drains are all everyday examples of thin, surface-associated groups of bacterial communities called biofilms. These microbial groups are composed of bacterial cells embedded within a self-produced extracellular matrix (ECM) that provides the biofilm with mechanical integrity and serves to protect the bacterial community from environmental stressors. Biofilms are ubiquitous and are implicated in a variety of medical and industrial problems, such as infections from implanted medical devices and the fouling of pipes and ships' hulls.[1–3] The bacterium *Pseudomonas aeruginosa* exists as biofilms in lungs of patients with cystic fibrosis,[4] in patients with chronic wounds,[5,6] and is the most common bacterium causing ventilator-assisted pneumonia,[7] which can arise or be sustained from biofilms forming upon endotracheal tubes.[8,9] These biofilms can be persistent and difficult to eradicate. Antibiotics that are effective against individual bacterial cells often do not affect these communities of cells.[10] Yet biofilms can also have beneficial purposes and can aid in the remediation of wastewater, soil, or gasoline spills, and protect agricultural crops.[11–13]

In the laboratory, biofilm colonies are traditionally grown on the surface of agar plates at the gel–air interface, as pellicles at the liquid–air interface, or in well plates at the solid–liquid interface. These growth methods have been invaluable in contributing to our current understanding of both biofilms themselves and microbial behavior. However, conventional culturing protocols can have limitations, and

Prof. C. B. Chang, Prof. J. N. Wilking, Prof. S.-H. Kim, Prof. H. C. Shum, Prof. D. A. Weitz
School of Engineering and Applied Science
Department of Physics
Harvard University
Cambridge, MA 02138, USA
E-mail: weitz@seas.harvard.edu
Prof. C. B. Chang, Prof. J. N. Wilking
Chemical and Biological Engineering Department
Montana State University
Bozeman, MT 59717, USA
Prof. S.-H. Kim
Department of Chemical and Biomolecular Engineering
Korea Advanced Institute of Science and Technology
Daejeon 305-701, Korea
Prof. H. C. Shum
Department of Mechanical Engineering
The University of Hong Kong
China

DOI: 10.1002/smll.201403125

thus nonconventional techniques for creating customized microenvironments for bacterial growth have been developed, including micromachined cavities,[14–16] microfluidic flow cells,[17–20] and microchemostats.[21–24] These customized microenvironments have led to new insights into the microbial world: of persistence in bacterial subpopulations,[25] of the acceleration and emergence of bacterial antibiotic resistance,[14,26] of quorum sensing and cell-to-cell signaling.[15,27,28] Novel cultivation methods for microorganisms will continue to further our understanding of bacterial behavior and have the potential to transform the field of modern microbiology.[29–31]

Despite the power of these techniques, they cannot address the need for the creation of extremely large numbers of identical microenvironments necessary for high-throughput screening. Multiwell microtiter plates are utilized for studies that require analysis of numerous colonies; yet even multiwell plates can be limited by the number of samples that can be processed in a given period of time and space. One technique that can be used to perform large numbers of quantitative experiments in a short amount of time is drop-based microfluidics, in which drops from femtoliters to nanoliters in volume serve as tiny microreactor containers that can be used for high-throughput biological screening and assaying. Microfluidics provides a platform for the creation of immense numbers of monodisperse, microscopic drops and affords control over drop size and structure that is not accessible using bulk methods. Drop-based microfluidics has been previously utilized to study properties of single bacterial cells,[32–35] and green fluorescent protein (GFP) expression from many cells;[36] however, the formation of communities of bacteria such as biofilms in drops has not been previously explored. Growth of biofilm communities in drops would allow for the vast application of microfluidic technology; examples could include the screening of antibiotic drug conditions for the eradication of biofilms, or the large-scale exploration of growth conditions for culturing previously unculturable bacteria or biofilms.[37,38] As biofilms cause billions of dollars of damage each year in medicine and in industry,[39] high-throughput screening and applications that allow for a better understanding of biofilm formation and eradication can have enormous impacts on cost control and health improvement.

Here we demonstrate a new method for the cultivation of bacterial biofilms in emulsion drops. This is the first demonstration of drop-based microfluidic technology for the creation of multiple, monodisperse emulsion drops that serve as microenvironments for the containment and growth of bacterial biofilms. We show that the size of these drops allows analysis of colony heterogeneity and spatial–temporal structure of subpopulations. The ability of biofilms to form in emulsion drops makes the encapsulated samples amenable to rapid manipulation and analysis using current high-throughput microfluidic techniques.

2. Results and Discussion

To create multiple, monodisperse double emulsion drops, we use a glass capillary microfluidic device to create water-in-oil-in-water (w/o/w) drops by coflowing coaxial streams of water in oil and using hydrodynamic flow-focusing of a third outer stream of water to generate individual drops (**Figure 1**A). This device can create monodisperse drops at rates of 100–5000 Hz and with well-defined diameters between 20 and 300 μm.[40] The thickness of the oil shell can be tuned by varying the relative flow rates of the liquids and can be made as thin as a few micrometers. Multiple monodisperse drops can be created with this device (Figure 1C).

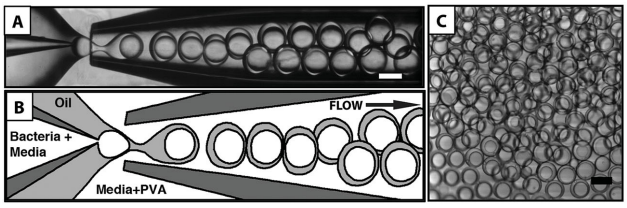

Figure 1. A) Microscale w/o/w double emulsions are created using a flow-focusing glass-capillary microfluidic device, in which bacteria and media are coflowed with oil to produce 20–300 μm diameter double emulsion drops. Image taken using a high-speed camera. B) Schematic of the flow-focusing region with the liquid compositions labeled. C) Microscopy image of multiple monodisperse double emulsion drops created with the microfluidic device. Scale bars correspond to 200 μm.

We use *Bacillus subtilis*, a model organism for studying biofilms. A Gram-positive soil bacterium, it undergoes several well-characterized developmental pathways of cellular differentiation. During biofilm formation on an agar surface, these cells follow a defined lineage where planktonic cells differentiate to matrix-forming cells and sporulating cells.[41] The promoter genes that are responsible for each of these cell phenotypes are fused with fluorescent proteins, enabling cellular differentiation to be observed using confocal microscopy.

We encapsulate an aqueous suspension of planktonic *B. subtilis* bacterial cells to create w/o/w double emulsion drops (Figure 1B) with an outer diameter of ≈164 ± 4 μm (see the Microfluidic Device Operation section). Within 24 h, these planktonic cells multiply and differentiate into matrix-forming cells at the inner interface of these microscopic drops, forming 3D spherical biofilms on the inside of the oil shells. The inner water–oil (w/o) interface is stabilized with a silicone surfactant, which is a known film-former, and provides a substrate upon which the biofilm readily adheres; moreover, the small size of these drops makes them amenable to analysis. In Figure 1C, we picture only a very small subset of the total drops made in a typical experiment. For these experiments, approximately 300 000 double emulsion drops were created in only 10 min of drop collection (see the ($W_1/O_1/W_2$) Double Emulsion Composition section).

We are able to follow the growth and development of *B. subtilis* biofilms over time, following gene expression of the bacteria as they undergo differentiation from swimming to matrix-forming. We use a dual-labeled reporter of the bacteria that expresses cyan fluorescent protein (CFP) when swimming and yellow fluorescent protein (YFP) when matrix-forming (**Figure 2**A). The planktonic bacteria localize and multiply at the inner w/o liquid interface (cyan bacteria, Figure 2B). Within the first 12 h, the bacterial cells

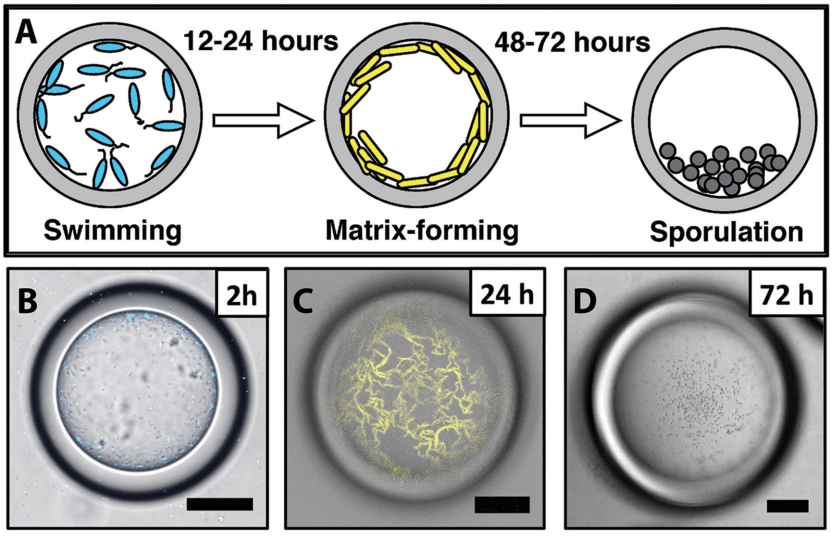

Figure 2. A) Illustration of dual-labeled *B. subtilis* 3610 bacteria (*amyE::*P_{tapA}*-yfp, lacA::*P_{hag}*-cfp*) differentiating within a w/o/w double emulsion drop. The majority of bacterial cells are planktonic during the first few hours, differentiate into matrix-forming cells while losing their flagella between 12 and 24 h, and transition into spores between 48 and 72 h. B–D) Micrographs of *B. subtilis* biofilm differentiation within drops taken using confocal microscopy. B) At 2 h, most cells express blue fluorescence, indicating motility (P_{hag}-cfp, where *hag* encodes flagellin). The image plane is in the middle of the drop. C) At 24 h most cells have differentiated into matrix-producing cells and a robust biofilm is formed on the inner interface of the double emulsion drop. The image is taken near the bottom of the drop to capture the 2D structure. D) At 72 h spherical nonfluorescent endospores appear and collect at the bottom of the double emulsion drop, where the image is taken. All scale bars correspond to 50 μm.

differentiate from rod-shaped, motile swimmers to elongated chains of nonmotile, matrix-forming cells at the interface. A ropey biomass structure appears throughout the entire inner drop interface (yellow bacteria, Figure 2C, and Movie in the Supporting Information). This ropey microstructure is similar to the microstructure observed in *B. subtilis* pellicles,[42] which form at air–water interfaces; in both cases, the biofilm grows in direct contact with a reservoir of water. After 48 h, some of the matrix-forming cells differentiate into spores, resulting in a mixture of matrix-forming cells and spores. After 72 h, all of the matrix-producing cells have sporulated (nonfluorescent bacteria, Figure 2D). These endospore cells are no longer capable of producing exopolysaccharides (EPS) and amyloid fibers from TasA proteins, the two major components of the biofilm ECM. Thus, they sink to the bottom of the drop and are unable to remain adhered to the w/o interface. A control experiment of *B. subtilis* 3610 in Luria Bertani (LB) media does not form biofilm at the interface after one day (Figure 7A).

To characterize differentiation from planktonic to matrix forming, we measure the average intensities of the fluorescent reporters within the drops, and plot these as a function of time. We find that the overall intensity of the matrix reporter within an individual drop increases dramatically, by nearly an order of magnitude, in the first 12 h. By contrast, the intensity of the swimming reporter increases by only a factor of two over this same time period (**Figure 3**A). We hypothesize that the increase in the swimming reporter intensity is due to an overall increase in the number of bacteria and the increase in the matrix-production intensity is due to a shift in the overall population type at the onset of biofilm production. We note that this is a semiquantitative result. Truly quantifying the two populations would require integrating the intensity in the entire drop, correcting for autofluorescence and correcting for any overlap between emission spectra. Nevertheless, qualitatively similar behavior has been observed in biofilms grown on agar, where bacteria differentiate from swimming to matrix-forming,[41] as well as in a recent study, which demonstrates that nutrient depletion triggers matrix production in *B. subtilis* biofilms.[43] The peak in matrix-production of wild-type *B. subtilis* in drops occurs at 12 h. This timescale is consistent with our observations of *B. subtilis* aggregation in liquid cultures and occurs slightly earlier than observed for wild-type *B. subtilis* biofilms grown on agar (Figure 3A).[44]

We observe an overall decrease in drop size as the biofilm grows (Figure 3B). The calculated inner water volume decreases by 45% over the first 12 h and then remains constant (Figure 3C). This corresponds to the peak in matrix-production (Figure 3A). In addition, when encapsulating a very dilute concentration of bacteria so that only a few of the drops contain bacteria, drops that contain bacteria shrink compared to those with only media in the inner phase (**Figure 4**A). Thus, this decrease in volume can be attributed to nutrient depletion, which creates an osmotically driven water flux from the inner aqueous phase to the outer continuous phase; this can occur because of a very small, but nonzero solubility of water in the silicone oil used (40 mol m^{-3} at 21 °C).[45] This is consistent with a previous study of active coarsening between drops containing yeast cells and empty drops; bioactivity of the yeast cells lowered overall solute concentrations within those drops, causing them to shrink while the neighboring empty drops swelled.[46] By contrast to the single emulsions, for the double emulsions there is no evidence of water transfer from one drop to another. Instead, there is only transfer to the continuous phase, which serves as a reservoir for water.

While there is flux of water through the oil shell of the double emulsions, there is no flux of nutrient. We grow biofilms in double emulsion drops with roughly similar inner volume, but of different shell thicknesses. Independent of shell thickness, the biofilm grows to the about the same thickness in the drops, ≈5–10 μm, as shown in the series of images in Figure 4C. This suggests that there is no flux of nutrient, even through the thinnest shells. This is in contrast to the observed flux of water through the shell, upon osmotic pressure mismatch between the inner and continuous phases.

We also explore the formation of the biofilms in inverse w/o single emulsions (see the (W_1/O_1) Single Emulsion Composition section). The outer oil phase is a fluorinated oil

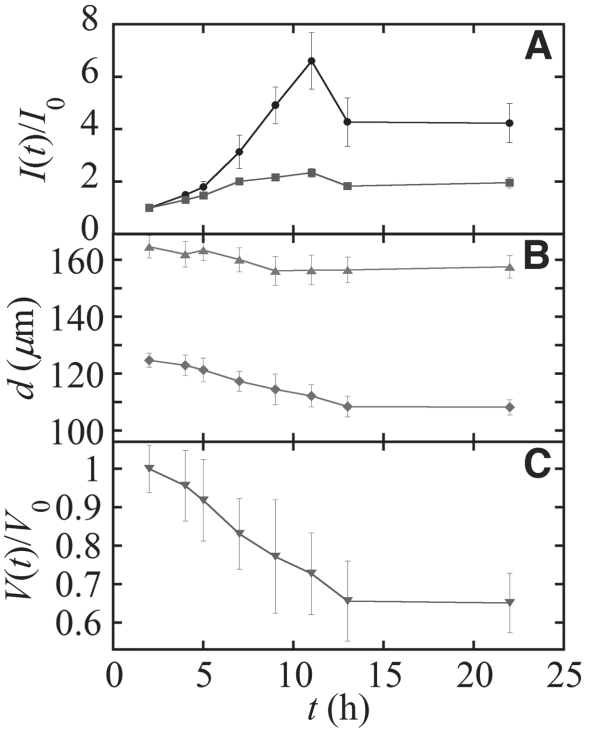

Figure 3. A) Average intensity per drop, $I(t)$, normalized by the initial intensity, I_0, and plotted as a function of time for drops containing dual-labeled *B. subtilis* 3610 bacteria (*amyE::*P_{tapA}*-yfp, lacA::*P_{hag}*-cfp*) with fluorescently labeled promoter genes that correspond to swimming (squares, ■) and matrix production (circles, ●). B) Plot of average inner diameter (diamonds, ◆) and outer diameter (upward triangles, ▲) of the double emulsion drops over time. C) Average drop volume $V(t)$, normalized by the initial volume, V_0, plotted over time (downward triangles, ▼).

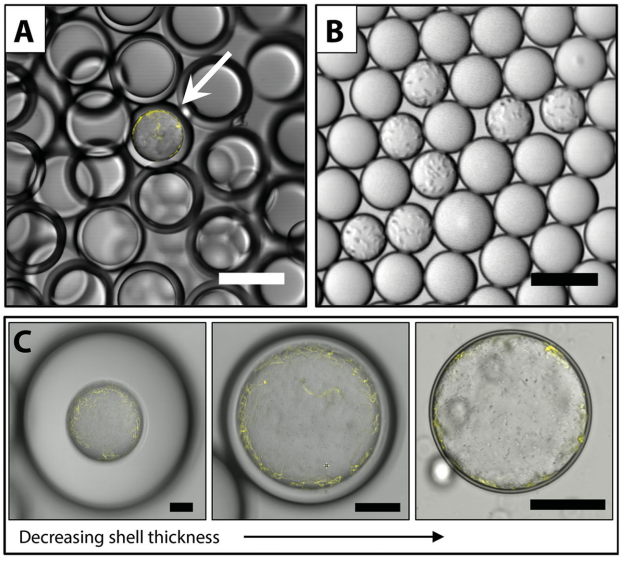

Figure 4. A) A double emulsion drop containing a mature biofilm (white arrow) is smaller in size (inner diameter, d = 276 μm) than the empty, surrounding drops (average inner diameter, $\bar{d}$ = 307 ± 8 μm), indicating that water has passed through the oil shell. B) Likewise, single emulsion w/o drops containing bacteria shrink, while the empty, surrounding drops swell. C) Varying oil shell thicknesses. *B. subtilis* 3610 cells expressing an accessory protein component of the ECM, TapA, form a ropey biomass indicative of biofilm structure at the inner water–oil interface after 24 h at room temperature, regardless of the thickness of the outer shell. Scale bar in A corresponds to 200 μm. Scale bar in B corresponds to 25 μm. Scale bars in C correspond to 50 μm.

with 1% (w/v) fluoro-PEG-ylated surfactant.[47] We use sizes ranging from 20 to 200 μm in diameter. For all w/o emulsions, clumps of biofilm-forming bacteria are seen; however, biofilms do not form at the liquid–liquid interface due to the specific combination of the oil and surfactant. This is likely due to the poly(ethylene glycol) (PEG) at the interface, upon which biological agents, such as proteins, cells and enzymes, do not typically adhere. Similar to the double emulsions (Figure 4A), we also observe active coarsening[46] in single emulsions, where drops containing bacteria shrink while empty drops swell (Figure 4B).

Thus, the double emulsion system is comprised of a suitable combination of volume and surface chemistry for biofilm growth. The double emulsions are not so small as to limit biofilm formation due to insufficient nutrient; moreover, the surfactant (DC749) is a known film-forming silicone that presumably creates a conditioning film for the biofilm.

Oxygen permeability in both of the oils used in the single (HFE-7500) and double emulsions (10cSt DC200 polydimethylsiloxane (PDMS) silicone oil) is high. The permeability of oxygen in silicone oil is 4.1×10^{-5} cm^2 s^{-1}[48] and 5.61×10^{-5} cm^2 s^{-1}[49] in perfluorocarbon oil (compared to 2.78×10^{-5} cm^2 s^{-1} in water).[49] In both cases, the drops rise to liquid–air interface, allowing the biofilms to be exposed to oxygen in the air.

Microfluidic techniques allow facile manipulation of liquid interfaces, and we exploit this by directing biofilm growth upon specific surfaces in a triple emulsion system (o/w/o/w) and in a double emulsion system of inverse composition (o/w/o) (see the (O_1/W_1/O_2) Double Emulsion Composition and (O_1/W_1/O_2/W_2) Triple Emulsion Composition sections). In these systems, the choice of surfactants in the aqueous and oil phases both stabilize the liquid interfaces and direct the growth of biofilms upon preferential interfaces. When bacteria are encapsulated in the inner aqueous phase of a triple (o/w/o/w) emulsion, we find that the bacteria preferentially forms a biofilm on the inner oil interface, even at the expense of a closer proximity to an oxygen source as is the case for the outer oil interface (**Figure 5**A). Notably, the biofilm on the inner oil interface is positive in curvature. This is in contrast to the (w/o/w) double emulsion system, in which the biofilm prefers the outer oil shell of negative curvature. Thus, we show that biofilms can be formed upon interfaces with both negative and positive radii of curvature by adjusting the surfactant and oil composition. In fact, we show that it can form on the inner drop of inverse double emulsion composition (o/w/o) (Figure 5B). The biofilm forms upon the inner oil phase of positive curvature, not upon the PEG-ylated interface, consistent with the inverse w/o single emulsions. Therefore, we can fine-tune the liquid–liquid interfaces in order to design higher-order multiple emulsions for preferential biofilm attachment. For both the triple and inverse double emulsion, we observe that the structure of the

www.MaterialsViews.com

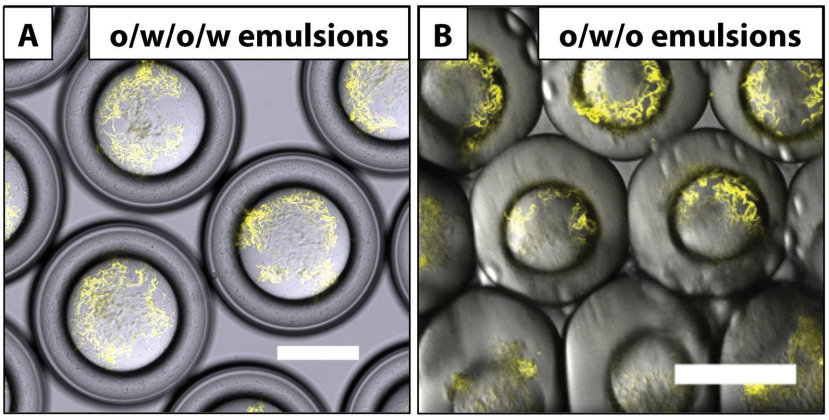

Figure 5. A) Triple emulsions of o/w/o/w are created using glass capillary microfluidics. B) Double emulsions of o/w/o. The biofilm preferentially grows on the inner oil drop in both cases. Scale bar in A corresponds to 100 μm. Scale bar in B corresponds to 200 μm.

biofilm and the timescale associated with biofilm formation are similar to that for double emulsions.

To better understand biofilm adhesion to the interfaces of the drops, we compare the structure of wild-type *B. subtilis* biofilms in drops to the structure of matrix mutants in drops (**Figure 6**). The two primary components of the *B. subtilis* ECM are EPS and a protein TasA that is known to form amyloid fibers.[50] We use three different *B. subtilis* mutants defective in the genes responsible for these essential biofilm components: Δ*tasA*, Δ*eps,* and the double Δ*tasA*Δ*eps* gene knockouts. In addition, we use a Δ*hag* mutant that cannot produce flagella to determine the role of swimming motility in surface coverage formation in the drops. When either of the matrix components are missing, distinct ropey biofilm is absent at the inner drop interface; the Δ*eps* bacteria has weak clumps of bacteria at the interface while the Δ*tasA* bacteria has a homogenous distribution of cells throughout the entire drop. In the Δ*tasA*Δ*eps* double knockout, all the cells are localized at the bottom of the drop and no biofilm is seen at the interface. Therefore, only the wild-type bacteria create a matrix that is seen on the entire inner interface. The results are strikingly similar to biofilms of these mutants grown as pellicles at the liquid–air interface;[51] the Δ*tasA* mutant makes flat pellicles, the Δ*eps* mutant makes a fragile, flat pellicle, and the double mutant makes no pellicles. In addition, we encapsulate a flagella mutant with no deficiency in matrix production. We find that the cells are unable to swim to interfaces throughout the drop, and biofilm production occurs only on the bottom half of the drop, where cells are initially localized due to gravity. Confocal micrographs of drops containing each of these mutants (Figure 6) show that the drop system is comparable to traditional liquid culturing of biofilm pellicles.

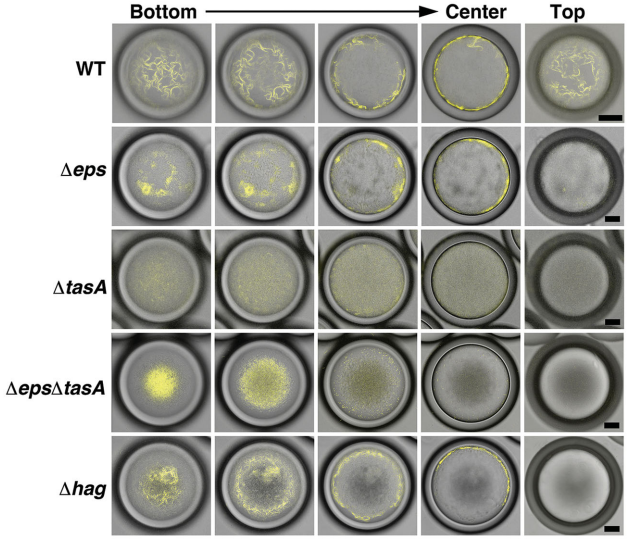

Figure 6. Cross-sectional images of double emulsion drops containing wild-type *B. subtilis* biofilm and *B. subtilis* biofilm mutants, taking using confocal microscopy after 24 h at 30 °C. The first four images in each row, from left to right, correspond to a series of images taken from the bottom of the drop to the center. The right-most column corresponds to images taken from the top of the drops. All cells in this figure contain a fluorescent reporter that is expressed in concert with an accessory protein component of the ECM, TapA (P_{tapA}-*yfp*), so the yellow fluorescence arises from matrix producing cells. (First row) Only the wild-type bacteria create a matrix that is seen on the entire inner interface. By contrast, the Δ*eps*, Δ*tasA*, and double Δ*eps*Δ*tasA* mutants lack components of the matrix and cannot form a robust biofilm on the inner interface of the drops. The flagella Δ*hag* mutant cannot swim but is not deficient in matrix-production; thus, biofilm is only seen on the bottom half of the drop. Scale bars correspond to 50 μm.

Finally, to demonstrate that this method of creating monodisperse drop environments for biofilm growth is not limited to a particular strain of bacteria, we grow *P. aeruginosa* PA14 biofilms in the drops. This species is known to form biofilms in Tryptone Broth (TB), but not in LB broth. This phenomenon is also seen in w/o/w double emulsions (**Figure 7**B vs C). A control strain of a mutant defective in biofilm formation, Δ*pelA,* does not form biofilm at the interface in TB, but instead behaves similarly to bacteria in LB (Figure 7D). This indicates that the drop environment can be applicable for other biofilm-forming bacteria.

3. Conclusion

In this work, we have demonstrated a number of different 3D interfaces for biofilm growth, which can be easily optimized for many biofilm species due to the availability of a wide variety of liquid materials and surfactants that one can use to fine-tune biofilm adhesion, shell permeability, and to either isolate, protect, or expose the cells to the surrounding environment. We find that PEG-ylated surfactants can prevent biofilms from attaching to drop interfaces, whereas neutrally charged, film-forming surfactants can provide a preferential surface for biofilm attachment. Interestingly, we observe that polyvinyl alcohol, a neutral, water-soluble surfactant, provides the most attractive surface. Biofilm extracellular polymeric substances (EPS) are typically anionic, yet their chemical composition can vary. Surfactants may be

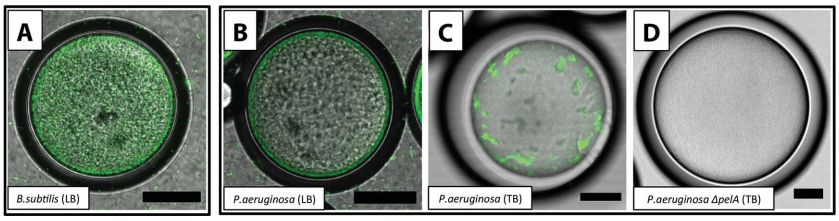

Figure 7. A) Constitutively labeled *B. subtilis* does not form a biofilm in LB broth, as expected. A homogeneous distribution of cells are seen at the interface, showing the lack of biofilm formation at the interface. B) Likewise, constitutively labeled *P. aeruginosa* does not form a biofilm in LB broth. Preferential localization of bacteria near the wall may possibly be due to aerotaxis, chemotaxis or weak, attractive surface interactions. C) By contrast, constitutively labeled *P. aeruginosa* does form a biofilm in TB broth. Aggregates of cells are seen at the interface, signifying biofilm formation at the interface. D) In TB broth, the Δ*pelA* mutant of *P. aeruginosa*, which cannot form the Pel polysaccharide of the matrix, does not form a biofilm at the liquid interface (strain is not fluorescent). All images are taken after 24 h at 30 °C. Scale bars correspond to 50 μm.

functionalized to allow specific binding to biofilm EPS. The oils used in this work were chosen for their biocompatibility and high oxygen solubility. Other oils or even porous solids could be used to allow the transport of specific chemicals and nutrients across the shell.

For the drops reported here, with sizes on the order of 100 μm, the biofilm conforms to the curvature of the drop. However, for smaller drops, geometric constraints imposed by the drops may modify the biofilm structure or surface coverage. Adherence to the inner interface of the drop could be prevented by the bending rigidity of the biofilm or individual bacterial bundles, thus altering surface coverage and biofilm structure. A systematic study of how geometric constraints modify biofilms structure would provide insight into biofilm mechanics.

Biofilm growth in 3D culture may have advantages over traditional 2D culture, such as increased diffusivity and transport of nutrients and may provide a more realistic *in vitro* model for biofilm growth occurring in 3D extracellular environments. These drop microenvironments for biofilm formation can aid in understanding inter- or intraspecies behavior of cell populations in confined environments, giving insight into the social behavior of cells, including how biofilms initially form, or how emergent behavior might arise from a complex population, such as antibiotic resistance in initial colony formation. In particular, these drop microenvironments for biofilm formation will enable the use of microfluidic technology to process greater numbers of biofilm samples, increasing the speed and throughput of existing state-of-the-art biofilm assays and revolutionizing current methods of biofilm screening.

In drop-based microfluidic screening assays, drop conditions can be detected using fluorescence and then sorted through the application of an electric field.[52–55] In this manner, drops can be rapidly sorted at kHz rates. To apply such detection and sorting methods to our biofilm microenvironments, a generic method of detecting biofilm formation would need to be established. This could be done using fluorescence,[52–55] through a fluorescent reporter for biofilm formation, or with fluorescent lectins that preferential bind and localize on the EPS. Biofilm formation could also be detected with static or dynamic light scattering. Due to its high sensitivity, scalability, and small sample volumes, drop-based microfluidics is well suited for the high-throughput study of these important questions in biofilm formation as well as for the advancement of biofilm science.

4. Experimental Section

Bacteria Strains and Culture: For all experiments, bacteria from freezer stocks are streaked onto a 1.5% agar LB medium plate. The plate is incubated for 12 h at 37 °C. An isolated colony from the plate is grown in 3 mL of liquid LB at 37 °C until the optical density (OD) at 600 nm reaches 1.0. The bacterial solution is then diluted to an OD of 0.1 in biofilm forming media of either MSgg[56] for *B. subtilis* NCIB3610 or TB for *P. aeruginosa* PA14 (10 g of BD Biosciences Bacto Tryptone in 1 L of water). The bacteria strain used in Figure 2–5 is the dual-labeled *B. subtilis* NCIB3610 *amyE::*P_{tapA}*-yfp, lacA::*P_{hag}*-cfp*, which expresses cyan fluorescent protein (cfp) when flagella genes are expressed (and cells are swimming) and yellow fluorescent protein (yfp) when matrix-producing genes are expressed.[41] In Figure 6, WT corresponds to the same dual-labeled strain described above, Δ*eps* corresponds to the matrix mutant *B. subtilis* NCIB3610 *epsA-O::tet, amyE::Pspac*^{c}*gfp* (spc) (HV1185), Δ*tasA* corresponds to the matrix mutant *B. subtilis* NCIB3610 *epsA-O::tet amyE::Pspac*^{c}*gfp* (spc) (HV1184), Δ*eps*Δ*tasA* corresponds to *B. subtilis* NCIB3610 *eps::tet, tasA::kan, amyE::*P_{tapA}*-yfp* (spc) (HV1250), and Δ*hag* corresponds to NCIB3610 *amyE::*P_{hag}*-cfp* (HV1152B). The Δ*tasA* (HV1184) and Δ*eps* (HV1185) knockouts were generated by using SPP1 phage-mediated generalized transduction[32,57] to transfer the *amyE::Pspac*^{c}*gfp* (spc) from strain EG219[56] to HV1173 (NCIB 3610 *tasA::kan*) or HV1182 (NCIB 3610 *epsA-O::tet*). Strains of *P. aeruginosa* include constitutively fluorescent *P. aeruginosa* PA14, and *P. aeruginosa* PA14 Δ*pelA* (ZK3437 or LF42).[58]

Microfluidic Device Operation: For all experiments, drops are created using pressure-driven flow in syringe pumps (Harvard Apparatus). Drop formation is imaged using a fast camera (Vision Research Phantom V9). The drops are collected in a 20–30x excess of the inner media solution to match inner and outer solution osmolarity in double and triple emulsion drops. The drops are incubated at 30 °C to promote biofilm growth.

(W_1/O_1) Single Emulsion Composition: The inner aqueous phase, W_1, is a suspension of planktonic B. *subtilis* bacterial cells at a fixed OD of 0.1 in aqueous MSgg media.[56] The outer oil phase, O_1, is a fluorinated oil (HFE-7500 3M NOVEC Engineered Fluid) with a 1% (w/v) fluoro-PEG-ylated surfactant.[47] Drops with diameters between 20 and 200 μm are created using a flow-focusing, drop-making microfluidic device created using PDMS soft lithography.

($W_1/O_1/W_2$) Double Emulsion Composition: The inner aqueous phase, W_1, is a suspension of planktonic *B. subtilis* bacterial cells at a fixed OD of 0.1 in aqueous MSgg media. The middle oil phase, O_1, is a silicone oil with surfactant (10cSt DC200 PDMS with 2% (w/v) DC749). The outer aqueous phase, W_2, is MSgg media

with 10% (w/v) poly(vinyl alcohol) (PVA, 87%–89% hydrolyzed, Mw 13 000–23 000, Sigma-Aldrich). The glass capillary microfluidic device used to fabricate the double emulsions is made using two aligned tapered cylindrical capillaries, of outer diameter 1.00 mm, that are inserted into opposite ends of a square capillary with inner diameter of 1.05 mm.[40] The thinnest shell double emulsion (Figure 4C) is made using the technique described in Kim et al.[59] Double emulsion drops pictured in Figure 2 and Figure 6 were created at flow rates of 1800 μL h^{-1} (inner), 2100 μL h^{-1} (middle), and 6000 μL h^{-1} (outer). These flow rates correspond to drop creation at ≈468 Hz.

($O_1/W_1/O_2$) Double Emulsion Composition: The inner oil phase, O_1, is silicone oil (10cSt DC200 PDMS). The middle aqueous phase, W_1, is a suspension of planktonic *B. subtilis* bacterial cells at a fixed OD of 0.1 in aqueous MSgg media containing 5% (w/v) PVA (87%–89% hydrolyzed, M_w 13 000–23 000, Sigma-Aldrich). The outer oil phase, O_2, is a fluorinated oil (HFE-7500 3M NOVEC Engineered Fluid) with a 1% (w/v) fluoro-PEG-ylated surfactant.[47] These double emulsions are also made using a glass capillary microfluidic device, as previously described.[40]

($O_1/W_1/O_2/W_2$) Triple Emulsion Composition: The inner oil phase, O_1, is 10cSt DC200 PDMS. The middle aqueous phase, W_1, is a suspension of planktonic *B. subtilis* bacterial cells at a fixed OD of 0.1 in aqueous MSgg media containing 5% (w/v) PVA (87%–89% hydrolyzed, M_w 13 000–23 000, Sigma-Aldrich). The outer oil phase, O_2, is 10cSt DC200 PDMS with 2% (w/v) DC749. The outer aqueous phase, W_2, is MSgg media with 10% (w/v) PVA (87%–89% hydrolyzed, Mw 13 000–23 000, Sigma-Aldrich). The triple emulsions are created using a one-step emulsification approach for making high-order monodisperse multiple emulsions drops.[60]

Confocal Microscopy and Image Analysis: Images in Figure 2– 7 are taken using a Leica TCS SP5 confocal laser scanning microscope with a 10x air objective (NA 0.30). The pinhole size is set at 1 Airy unit. The dual-labeled *B. subtilis* NCIB3610 *amyE::*P_{tapA}*-yfp, lacA::*P_{hag}*-cfp* is excited at 458 and 514 nm for CFP and YFP, with photomultiplier tube (PMT) detection ranges from 465 to 505 and 525 to 600 nm, respectively. A third PMT simultaneously collects a nonfluorescent image from 680 to 700 nm (reflection mode). In Figures 6 and 7, the *B. subtilis* Δ*eps*, Δ*tasA,* and *P. aeruginosa* strains are imaged using excitation at 488 nm for GFP with a PMT detection range from 500 to 600 nm. The Δ*eps*Δ*tasA* strain was imaged using excitation at 541 nm for YFP with a PMT detection range from 525 to 600 nm.

In Figure 3A, fluorescence intensities in the drops are analyzed using ImageJ.[61] The gain settings on the confocal microscope for each the two fluorescence channels (CFP and YFP) are consistent across all the time points, and do not oversaturate the PMTs. A circular region of interest is drawn to encircle an individual drop, in order to measure individual drop fluorescence in the each of the PMT channels. The number of drops, N, analyzed per time point ranges from N = 28–66. Error bars represent one standard deviation from the mean fluorescence intensity. Images displayed in all figures are minimally processed; only brightness and contrast is changed from the raw data.

The average, time-dependent inner drop diameter, $d(t)$, plotted in Figure 3B is used to calculate the average, time-dependent inner drop volume, $V(t)$, plotted in Figure 3C with $V(t) = (4\pi a^3)/3$, where $d = 2a$. V at t = 2h is taken as V_0 and volumes at each time point are normalized by V_0. $V(t)/V_0$ is then plotted as a function of time.

Supporting Information

Supporting Information is available from the Wiley Online Library or from the author.

Acknowledgements

This work was supported by the National Science Foundation (DMR-1310266), the Harvard Materials Research Science and Engineering Center (DMR-0820484), and the Office of Technology Development (OTD)-BASF Alliance. We also thank Hera Vlamakis and Roberto Kolter for the bacterial strains used in this paper and for insightful discussions.

[1] J. W. Costerton, P. S. Stewart, E. P. Greenberg, *Science* **1999**, *284*, 1318.
[2] M. W. LeChevallier, T. M. Babcock, R. G. Lee, *Appl. Environ. Microbiol.* **1987**, *53*, 2714.
[3] H. C. Flemming, *Appl. Microbiol. Biotechnol.* **2002**, *59*, 629.
[4] P. K. Singh, A. L. Schaefer, M. R. Parsek, T. O. Moninger, M. J. Welsh, E. P. Greenberg, *Nature* **2000**, *407*, 762.
[5] K. Kirketerp-Møller, P. Ø. Jensen, M. Fazli, K. G. Madsen, J. Pedersen, C. Moser, T. Tolker-Nielsen, N. Høiby, M. Givskov, T. Bjarnsholt, *J. Clin. Microbiol.* **2008**, *46*, 2717.
[6] M. Fazli, T. Bjarnsholt, K. Kirketerp-Møller, B. Jørgensen, A. S. Andersen, K. A. Krogfelt, M. Givskov, T. Tolker-Nielsen, *J. Clin. Microbiol.* **2009**, *47*, 4084.
[7] J. Chastre, J.-Y. Fagon, *Am. J. Respir. Crit. Care Med.* **2002**, *165*, 867.
[8] C. Adair, S. Gorman, B. Feron, L. Byers, D. Jones, C. Goldsmith, J. Moore, J. Kerr, M. Curran, G. Hogg, *Intensive Care Med.* **1999**, *25*, 1072.
[9] N. Safdar, C. J. Crnich, D. G. Maki, *Respir. Care* **2005**, *50*, 725.
[10] P. S. Stewart, J. W. Costerton, *Lancet* **2001**, *358*, 135.
[11] R. Singh, D. Paul, R. K. Jain, *Trends Microbiol.* **2006**, *14*, 389.
[12] A. B. Cunningham, R. R. Sharp, R. Hiebert, G. James, *Biorem. J.* **2003**, *7*, 151.
[13] Å. Kolmert, D. B. Johnson, *J. Chem. Technol. Biotechnol.* **2001**, *76*, 836.
[14] J. L. Connell, E. T. Ritschdorff, M. Whiteley, J. B. Shear, *Proc. Natl. Acad. Sci. USA* **2013**, *110*, 18380.
[15] J. L. Connell, A. K. Wessel, M. R. Parsek, A. D. Ellington, M. Whiteley, J. B. Shear, *MBio* **2010**, *1*, e00202.
[16] F. J. Hol, P. Galajda, K. Nagy, R. G. Woolthuis, C. Dekker, J. E. Keymer, *PLoS One* **2013**, *8*, e77042.
[17] K. Drescher, Y. Shen, B. L. Bassler, H. A. Stone, *Proc. Natl. Acad. Sci. USA* **2013**, *110*, 4345.
[18] R. Rusconi, S. Lecuyer, N. Autrusson, L. Guglielmini, H. A. Stone, *Biophys. J.* **2011**, *100*, 1392.
[19] R. Rusconi, S. Lecuyer, L. Guglielmini, H. A. Stone, *J. R. Soc. Interface* **2010**, *7*, 1293.
[20] P. Wang, L. Robert, J. Pelletier, W. L. Dang, F. Taddei, A. Wright, S. Jun, *Curr. Biol.* **2010**, *20*, 1099.
[21] F. K. Balagaddé, L. You, C. L. Hansen, F. H. Arnold, S. R. Quake, *Science* **2005**, *309*, 137.
[22] J. R. Moffitt, J. B. Lee, P. Cluzel, *Lab chip* **2012**, *12*, 1487.
[23] Z. Long, E. Nugent, A. Javer, P. Cicuta, B. Sclavi, M. C. Lagomarsino, K. D. Dorfman, *Lab Chip* **2013**, *13*, 947.
[24] A. Groisman, C. Lobo, H. Cho, J. K. Campbell, Y. S. Dufour, A. M. Stevens, A. Levchenko, *Nat. Methods* **2005**, *2*, 685.

[25] N. Q. Balaban, J. Merrin, R. Chait, L. Kowalik, S. Leibler, *Science* **2004**, *305*, 1622.
[26] Q. Zhang, G. Lambert, D. Liao, H. Kim, K Robin, C. K. Tung, N. Pourmand, R. H. Austin, *Science* **2011**, *333*, 1764.
[27] S. T. Flickinger, M. F. Copeland, E. M. Downes, A. T. Braasch, H. H. Tuson, Y.-J. Eun, D. B. Weibel, *J. Am. Chem. Soc.* **2011**, *133*, 5966.
[28] J. Q. Boedicker, M. E. Vincent, R. F. Ismagilov, *Angew. Chem. Int. Ed. Engl.* **2009**, *48*, 5908.
[29] A. K. Wessel, L. Hmelo, M. R. Parsek, M. Whiteley, *Nat. Rev. Microbiol.* **2013**, *11*, 337.
[30] J. L. Connell, M. Whiteley, J. B. Shear, *Nat. Chem. Biol.* **2012**, *8*, 10.
[31] F. J. Hol, C. Dekker, *Science* **2014**, *346*, 1251821.
[32] P. R. Marcoux, M. Dupoy, R. Mathey, A. Novelli-Rousseau, V. Heran, S. Morales, F. Rivera, P. L. Joly, J.-P. Moy, F. Mallard, *Colloids Surf. A* **2011**, *377*, 54.
[33] J. Q. Boedicker, L. Li, T. R. Kline, R. F. Ismagilov, *Lab Chip* **2008**, *8*, 1265.
[34] J.-C. Baret, O. J. Miller, V. Taly, M. Ryckelynck, A. El-Harrak, L. Frenz, C. Rick, M. L. Samuels, J. B. Hutchison, J. J. Agresti, D. R. Link, D. A. Weitz, A. D. Griffiths, *Lab Chip* **2009**, *9*, 1850.
[35] J.-U. Shim, L. F. Olguin, G. Whyte, D. Scott, A. Babtie, C. Abell, W. T. S. Huck, F. Hollfelder, *J. Am. Chem. Soc.* **2009**, *131*, 15251.
[36] Y. Zhang, Y.-P. Ho, Y.-L. Chiu, H. F. Chan, B. Chlebina, T. Schuhmann, L. You, K. W. Leong, *Biomaterials* **2013**, *34*, 4564.
[37] P. J. Turnbaugh, R. E. Ley, M. Hamady, C. Fraser-Liggett, R. Knight, J. I. Gordon, *Nature* **2007**, *449*, 804.
[38] K. Zengler, G. Toledo, M. Rappé, J. Elkins, E. J. Mathur, J. M. Short, M. Keller, *Proc. Natl. Acad. Sci. USA* **2002**, *99*, 15681.
[39] M. Chicurel, *Nature* **2000**, *408*, 284.
[40] A. S. Utada, E. Lorenceau, D. R. Link, P. D. Kaplan, H. A. Stone, D. A. Weitz, *Science* **2005**, *308*, 537.
[41] H. Vlamakis, C. Aguilar, R. Losick, R. Kolter, *Genes Dev.* **2008**, *22*, 945.
[42] K. Kobayashi, *J. Bacteriol.* **2007**, *189*, 4920.
[43] W. Zhang, A. Seminara, M. Suaris, M. P. Brenner, D. A. Weitz, T. E. Angelini, *New J. Phys.* **2014**, *16*, 015028.
[44] A. Seminara, T. E. Angelini, J. N. Wilking, H. Vlamakis, S. Ebrahim, R. Kolter, D. A. Weitz, M. P. Brenner, *Proc. Natl. Acad. Sci. USA* **2012**, *109*, 1116.
[45] G. C. Randall, P. S. Doyle, *Proc. Natl. Acad. Sci. USA* **2005**, *102*, 10813.
[46] L. Boitard, D. Cottinet, C. Kleinschmitt, N. Bremond, J. Baudry, G. Yvert, J. Bibette, *Proc. Natl. Acad. Sci. USA* **2012**, *109*, 7181.
[47] C. Holtze, A. C. Rowat, J. J. Agresti, J. B. Hutchison, F. E. Angile; C. H. J. Schmitz, S. Koster, H. Duan, K. J. Humphry, R. A. Scanga, J. S. Johnson, D. Pisignano, D. A. Weitz, *Lab Chip* **2008**, *8*, 1632.
[48] S. Charati, S. Stern, *Macromolecules* **1998**, *31*, 5529.
[49] R. Lanza, R. Langer, J. P. Vacanti, *Principles of Tissue Engineering*, Academic Press, Boston, **2014**.
[50] D. Romero, C. Aguilar, R. Losick, R. Kolter, *Proc. Natl. Acad. Sci. USA* **2010**, *107*, 2230.
[51] S. S. Branda, F. Chu, D. B. Kearns, R. Losick, R. Kolter, *Mol. Microbiol.* **2006**, *59*, 1229.
[52] J. J. Agresti, E. Antipov, A. R. Abate, K. Ahn, A. C. Rowat, J.-C. Baret, M. Marquez, A. M. Klibanov, A. D. Griffiths, D. A. Weitz, *Proc. Natl. Acad. Sci. USA* **2010**, *107*, 4004.
[53] J.-C. Baret, O. J. Miller, V. Taly, M. Ryckelynck, A. El-Harrak, L. Frenz, C. Rick, M. L. Samuels, J. B. Hutchison, J. J. Agresti, *Lab Chip* **2009**, *9*, 1850.
[54] E. Brouzes, M. Medkova, N. Savenelli, D. Marran, M. Twardowski, J. B. Hutchison, J. M. Rothberg, D. R. Link, N. Perrimon, M. L. Samuels, *Proc. Natl. Acad. Sci. USA* **2009**, *106*, 14195.
[55] L. Mazutis, J. Gilbert, W. L. Ung, D. A. Weitz, A. D. Griffiths, J. A. Heyman, *Nat. Protoc.* **2013**, *8*, 870.
[56] S. S. Branda, J. E. González-Pastor, S. Ben-Yehuda, R. Losick, R. Kolter, *Proc. Natl. Acad. Sci. USA* **2001**, *98*, 11621.
[57] R. E. Yasbin, F. E. Young, *J. Virol.* **1974**, *14*, 1343.
[58] L. Friedman, R. Kolter, *Mol. Microbiol.* **2004**, *51*, 675.
[59] S.-H. Kim, J. W. Kim, J.-C. Cho, D. A. Weitz, *Lab Chip* **2011**, *11*, 3162.
[60] S.-H. Kim, D. A. Weitz, *Angew. Chem. Int. Ed.* **2011**, *50*, 8731.
[61] C. A. Schneider, W. S. Rasband, K. W. Eliceiri, *Nat. Methods* **2012**, *9*, 671.

Received: October 22, 2014
Revised: March 13, 2015
Published online: May 8, 2015